JGR Space Physics

RESEARCH ARTICLE
10.1029/2019JA027204

Special Section:
Equatorial Aeronomy: New results from the 15th International Symposium on Equatorial Aeronomy (ISEA-15) and beyond

Height Variation of Gaps in 150-km Echoes and Whole Atmosphere Community Climate Model Electron Densities Suggest Link to Upper Hybrid Resonance

Gerald A. Lehmacher[1], Haonan Wu[1], Erhan Kudeki[2], Pablo M. Reyes[3], David L. Hysell[4], and Marco Milla[5]

[1]Department of Physics and Astronomy, Clemson University, Clemson, SC, USA, [2]Department of Electrical and Computer Engineering, University of Illinois at Urbana-Champaign, Urbana, IL, USA, [3]Center for Geospace Studies, SRI International, Menlo Park, CA, USA, [4]Earth and Atmospheric Sciences, Cornell University, Ithaca, NY, USA, [5]Jicamarca Radio Observatory, Instituto Geofísico del Perú, Lima, Peru

Key Points:
- Specific gaps and lines in the 150-km echo structure correspond to specific electron density contours
- The height of the gaps varies with season and solar activity
- Wide gaps where echoes are suppressed likely correspond to regions of double resonance conditions

Correspondence to:
G. A. Lehmacher,
glehmac@clemson.edu

Citation:
Lehmacher, G. A., Wu, H., Kudeki, E., Reyes, P. M., Hysell, D. L., & Milla, M. (2020). Height variation of gaps in 150-km echoes and Whole Atmosphere Community Climate Model electron densities suggest link to upper hybrid resonance. *Journal of Geophysical Research: Space Physics*, *125*, e2019JA027204. https://doi.org/10.1029/2019JA027204

Received 29 JUL 2019
Accepted 15 NOV 2019
Accepted article online 27 DEC 2019

Abstract Radar echoes from the daytime lower *F* region near the magnetic equator, so-called 150-km echoes, have been puzzling researchers for decades. Neither the mechanisms that generate the enhanced backscatter at very high frequencies (typically 30–50 MHz), the sharp lower cutoff height, the intricate layering with multiple echo layers separated by narrow gaps, nor the modulation of the echoes by short-period gravity waves is well understood. Here we focus on the diurnal variation of the echo layers—specifically, certain wide gaps in the vertical structure—which apparently descend in the morning, reach their lowest altitude near local noon, and ascend in the afternoon, sometimes described as necklace structure based on the appearance of the layers in range-time-intensity diagrams. Analyzing high-resolution data obtained with the Jicamarca radar between 2005 and 2017, spanning more than one solar cycle, we find that (a) wide gaps and narrow lines occur in vertically stacked, systematically repeating pattern; (b) the gap heights vary with season and solar cycle; and (c) the gap heights can be associated with specific contours of plasma frequencies or electron densities. The last two findings are supported by simultaneous observations of VIPIR ionosonde reflection heights and by comparison of gap heights with electron density contours obtained with the WACCM-X 2.0 global model. Finally, the wide gaps appear to coincide with the double resonance condition, where the upper hybrid frequency equals integer multiples of the electron gyrofrequency. This may explain why field-aligned plasma irregularities are suppressed and enhanced radar backscatter is not observed inside the gaps.

1. Introduction

Enhanced radar backscatter at very high frequencies (typically 30–50 MHz) from the daytime lower *F* region (F_1) near the magnetic equator, so-called 150-km echoes, have intrigued researchers for decades (Balsley, 1964; de Paula & Hysell, 2004; Choudhary et al., 2004; Kudeki & Fawcett, 1993; Kudeki et al., 1998; Li et al., 2013; Patra et al., 2008; Røyrvik & Miller, 1981). Neither the mechanisms causing enhanced backscatter between ~130 and ~180 km, the sharp lower cutoff height, the intricate structure with multiple echo layers separated by narrow and wide gaps, nor the modulation of the echoes by gravity waves with 10- to 15-min periods and very long vertical wavelengths are well understood. The echoes have been observed by many radars located at or near the magnetic equator (see references above). There are two types of echoes (Chau & Kudeki, 2013; Patra, 2011); the strongest are highly magnetic aspect sensitive and likely due to coherent scatter from field-aligned irregularities (FAIs), while the majority of echoes can also be observed with off-perpendicular beams with the characteristics of naturally enhanced incoherent backscatter (Chau, 2004, 2009).

Kudeki and Fawcett (1993) reported the first high-resolution measurements with the Jicamarca Radio Observatory including detailed height-time-intensity or range-time-intensity diagrams. We illustrate the salient features of the 150-km echo structure in Figure 1 obtained at Jicamarca on 14 April 2015. In this paper we focus on the diurnal variation of the many parallel echo layers—and specifically on the height of certain narrow lines and wider gaps in the vertical echo structure. The echo layers descend in the morning, reach

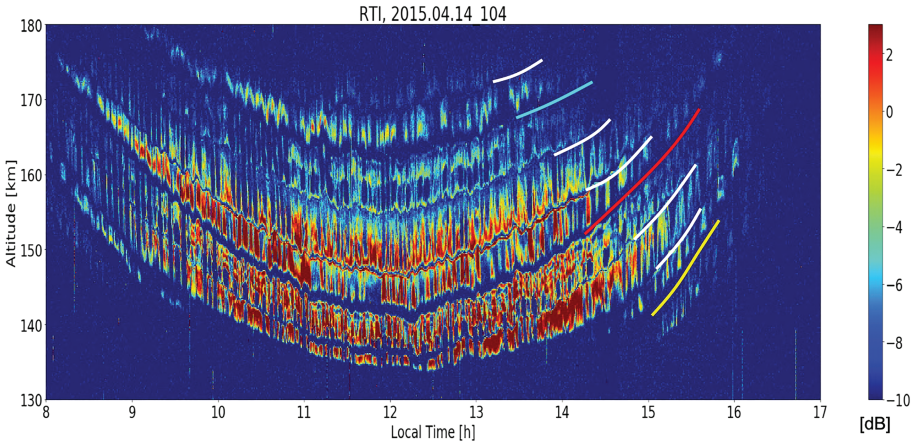

Figure 1. Height-time-intensity diagram of 150-km echoes from the Jicamarca vertical beam for 14 April 2015. Nominal range resolution is 150 m, and data were processed for 8.64-s time resolution. The color scale indicates the signal-to-noise ratio in dB. Systematically recurring wider gaps in the echo structure are marked with yellow, red, and cyan lines; narrower features in between the wide gaps are marked with white lines.

their lowest altitude near local noon, and ascend in the afternoon, which has been described as a necklace structure (Kudeki & Fawcett, 1993). We have (partially) marked three wider gaps with yellow, red, and cyan lines and narrow features with white lines. Throughout the day, all layers are almost coherently modulated by gravity waves with 10- to 15-min periods and very long vertical wavelengths. This can be best seen in the sinusoidal modulations of gaps and lines in the necklace, but also in the complex, quasiperiodic modulations of the backscatter signal.

Analyzing high-resolution data obtained with the Jicamarca radar between 2005 and 2017, spanning more than one solar cycle, we find that (a) wide gaps and narrow lines occur in vertically stacked, systematically repeating pattern; (b) the gap heights vary with season and solar cycle (meaning varying background ionization); and (c) the gap heights can be associated with specific contours of plasma frequencies or electron densities. Our findings are supported by simultaneous observations with the Vertical Incidence Pulsed Ionosphere Radar (VIPIR, an advanced ionosonde-dynasonde system) (Bullett et al., 2010) and by comparison of gap heights with electron density contours calculated with the WACCM-X 2.0 global atmosphere and ionosphere model (Liu et al., 2018).

Section 2 will briefly describe the radar and ionosonde measurements and model data. In section 3 we will compare VIPIR reflection heights with 150-km echo structures, and, using WACCM-X electron densities, we note for the first time the systematic variation of the gap heights with season and solar cycle. This strongly suggests that echo gaps and lines represent specific plasma frequency or electron density contours. In section 4 we explain that the estimated plasma frequencies of the wide gaps reflect the double resonance condition, that is, where the upper hybrid frequencies equal integer multiples of the electron cyclotron frequency ($f_{UH} = n \cdot eB/(2\pi m)$, with $n = 5, 6, 7, 8$). Section 5 contains our summary and conclusions.

2. Data

2.1. Radar Measurements

We used data acquired in the MST-ISR and MST-ISR-EEJ modes between 2005 and 2017 (Lehmacher et al., 2009, 2019). The Jicamarca radar is located near Lima, Peru (12°S, 75°W) at the magnetic dip equator and is the largest 50-MHz radar in the world. We used four Doppler beams perpendicular and a few degrees off with respect to the Earth's magnetic field (Reyes, 2017). Peak pulse power was typically 1.5 MW at 5% duty cycle and in the MST mode, we transmitted 64×1-μs complementary-code pulse pairs for a nominal vertical resolution of 150 m. Interpulse periods were typically 1.33 ms, and data were processed to yield Doppler spectra integrated over 1 min or less. Here we only use signal-to-noise ratio (SNR) which for 60-s spectra typically lies between −10 and 20 dB. Note that for 8.46-s spectra shown in Figure 1 the spectrally integrated SNR values are smaller. The radar collected data in this mode for several days per year since 2005, since fast, multichannel, digital data acquisition became available. Table 1 lists the days with high quality data used in this study.

Table 1
Jicamarca Radar Observations With High-Resolution MST Data Used in This Study

2005	2006/2007	2009	2014	2015	2016/2017
2005-03-15	2006-04-04	2009-01-17	2014-01-07	2015-01-06	2016-01-23[a]
2005-03-16	2006-04-05	2009-01-18	2014-01-08	2015-01-07	2016-01-24
2005-03-17	2006-04-06	2009-01-19	2014-01-09	2015-01-08	2016-01-25
2005-04-15	2006-08-01	2009-01-20	2014-01-10	2015-01-09	2016-01-26[a]
2005-04-27	2006-08-02	2009-01-21	2014-05-13	2015-04-07	2016-01-27
2005-06-13	2006-08-03	2009-01-22	2014-05-14	2015-04-14[a]	2016-01-28
2005-06-14	2006-09-05	2009-01-23	2014-05-15	2015-04-15[a]	2016-01-29
2005-06-15	2006-09-06	2009-01-24	2014-05-16	2015-04-16[a]	2016-01-30[a]
2005-06-16	2006-09-07	2009-01-25	2014-09-29	2015-04-17[a]	2016-01-31
2005-06-17	2006-12-05		2014-09-30	2015-07-07	2017-04-18
2005-09-06	2006-12-06		2014-10-01	2015-07-08	2017-04-19
2005-09-07	2006-12-07		2014-10-02	2015-07-09	2017-04-20
2005-09-08	2007-06-19			2015-07-10	
2005-12-13	2007-06-20			2015-09-29	
2005-12-14	2007-06-21			2015-09-30	
2005-12-20	2007-06-22			2015-10-01	
2005-12-21	2007-06-23			2015-10-02	
2005-12-22					

Note. Dates are formatted as YYYY-MM-DD.
[a]VIPIR data available for this study.

2.2. VIPIR Ionograms

The Vertical Incidence Pulsed Ionosonde Radar (VIPIR) is a versatile, advanced, multichannel digital ionosonde-dynasonde (Bullett et al., 2010). A VIPIR system has been installed at Jicamarca in 2008. It has a high dynamic range by direct digital radiofrequency sampling and high waveform agility allowing fast sweeps down to few seconds. The transmitter operates between 0.4 and 26 MHz with 4-kW peak power and 2% duty cycle. Eight receiver antennas and channels form north-south and east-west interferometers and allow for precise angle-of-arrival measurements for each echo. Here we use high-resolution ionograms, specifically virtual heights corresponding to the daytime lower F region with frequencies between 3 and 6 MHz. Stacked plots of virtual height versus time for different frequencies show short-period gravity wave activity that corresponds closely to the height modulations of the 150-km echoes (Reyes, 2017). These data are also discussed in detail in a separate manuscript that was recently submitted. Similar gravity wave modulations observed with the VIPIR system in Wallops Island, Virginia, have been analyzed by Negrea et al. (2016). From comparisons between VIPIR virtual heights and 150-km echoes we infer that specific gaps and lines in the necklace structure correspond to specific plasma frequencies and therefore local electron densities (see next section).

2.3. WACCM Model

We used electron densities calculated with the WACCM-X 2.0 model (Liu et al., 2010, 2018). The model extends from the surface to the upper thermosphere with a resolution of 1.9° in latitude, 2.5° in longitude, and 0.25 scale heights vertically. Upper atmospheric processes, including the transport of O^+, self-consistent ionospheric electrodynamics, and energetics included in WACCM-X are primarily based on the Thermosphere-Ionosphere-Electrodynamics General Circulation Model (TIE-GCM) (Roble et al., 1988; Richmond et al., 1992). The model was nudged (Smith et al., 2017) with specified dynamics up to 50 km from the National Aeronautics and Space Administration Modern Era Retrospective Analysis for Research and Applications version 2 Gelaro et al. (2017). The effects of a powerful (X17) solar flare on 7 September 2005 (Reyes, 2012) were recently modeled with WACCM-X. The modeled electron densities were compared with the response of the 150-km echoes during the flare as part of a separate publication (Pedatella et al., 2019). For this paper we use hourly output from a multiyear run (2002 to 2016) of WACCM-X 2.0 with specified dynamics. Solar flares and other transient energy inputs into the atmosphere-ionosphere systems are

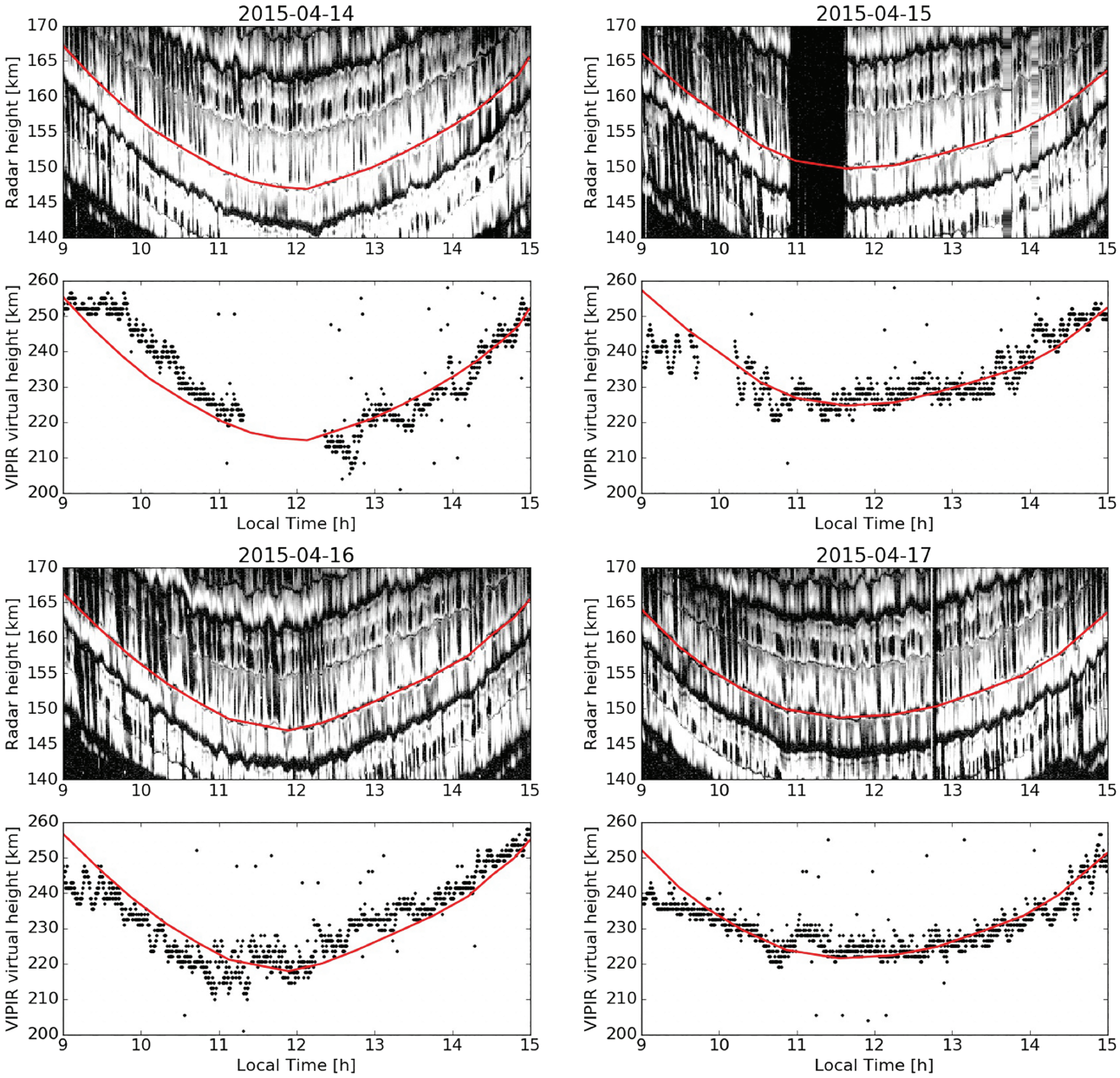

Figure 2. The 150-km necklace versus true height (top) and VIPIR 4.68 MHz versus virtual height (bottom) for 14–17 April 2015. The narrow necklace line above the wide gap is marked with red.

not considered; however, solar and geomagnetic variability is considered using sunspot number, $F_{10.7}$ flux, and a convection pattern based on the K_p index. For comparison with radar echoes, we have interpolated the modeled electron densities in time and geometric height and converted them to plasma frequency in MHz.

3. Observations

3.1. VIPIR Comparisons

In 2015 and 2016, the VIPIR ionosonde-dynasonde was operated on several days simultaneously with the radar and provided ionograms with 1-min resolution (see Table 1). Consecutive ionograms clearly show gravity wave activity throughout the ionosphere with similar periods as the modulation of 150-km echoes (Reyes, 2017). Reyes (2017) presents graphs of virtual height, $h(f,t) = c\tau/2$ versus local time for each transmitted frequency f. Each point on these graphs represents the virtual height where the transmitted frequency equals the local plasma frequency f_p, or equivalently, the local plasma density N, since

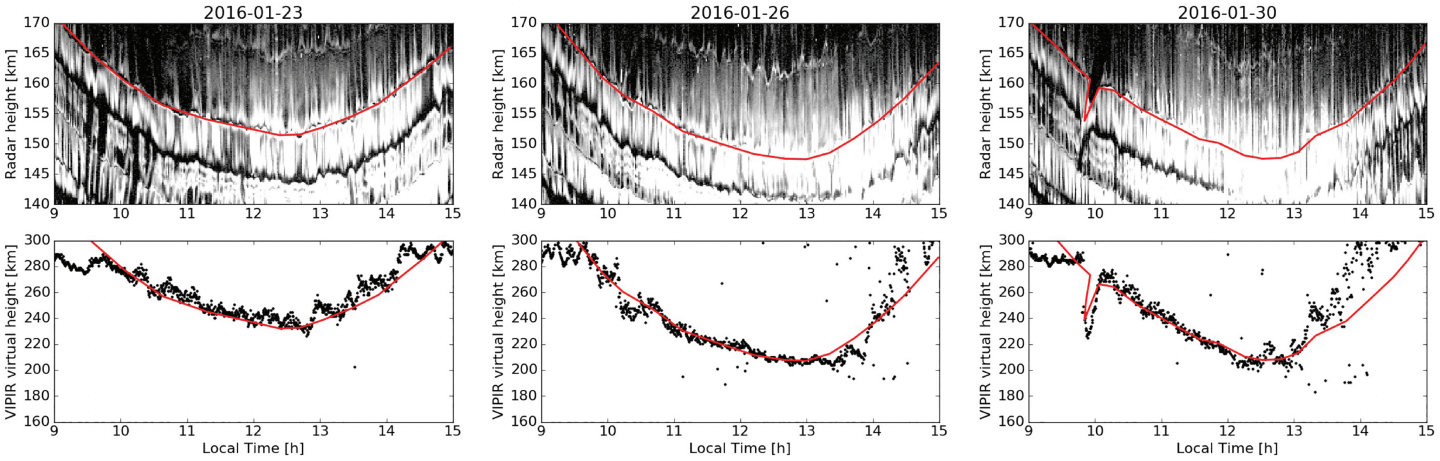

Figure 3. Same as previous figure, but for 23, 26, and 30 January 2016.

f_p [MHz] $\approx 8.97\sqrt{N\,[\mathrm{cm}^{-3}]}$. Since electron density increases in the morning and decreases in the afternoon, the graphs form a vertical stack of U-shaped electron density contours; typically electron density above 130 km increases monotonic with height. The valley region between E and F_2 layer (or F_1 layer if present) is characterized by plasma frequencies of 3 to 5 MHz (1.1 to 3.1 $\times 10^5$ cm^{-3}), depending on the level of ionization.

For data collected on 17 April 2015, Reyes (2017) compared the small-scale gravity wave modulations in the plasma frequency contours with wave modulations of the 150-km echoes. Specifically, he looked at a sharply defined line in the echoes around 150 km, which is always above a wide gap in the necklace pattern. In Figure 1 it is the first white line above the gap marked with red. It turns out that relative amplitudes and phases match the VIPIR plasma frequency contour best for $f_p = 4.68$ MHz. Reyes (2017) also found that for data between 13:00 and 14:30 LT the virtual height amplitude from VIPIR data is 4 times larger than the true height amplitude from the radar echoes. This indicates that the background electron density and gradient which determine the transmission time for the pulse and virtual height are relatively constant for a specific height and time interval.

Next, we looked at the same sharp feature, that is, the lines few kilometers above the "red" gap, in 150-km echoes for all available days with simultaneous VIPIR observations. Seven days (14, 15, 16, and 17 April 2015 and 23, 26, and 30 January 2016) were available for comparison (Figures 2 and 3). We find that the diurnal variation of plasma frequency contours for 4.68 MHz as observed with VIPIR resembles closely the variation of the necklace pattern in 150-km echoes. We also find that the virtual height variation at local noon is about 4 times larger than the true height variation (not shown) which is consistent with the variation for small wave amplitudes found by Reyes (2017). Based on these two results (the matching wave amplitude and the matching diurnal pattern), we strongly suggest that the well-defined narrow feature in the necklace is located where the local plasma frequency equals 4.68 MHz (electron density 2.72 $\times 10^5$ cm^{-3}).

3.2. Variation of Gap Heights

Now, there are many quasi-parallel necklace lines, both wide and thin gaps and narrow enhanced regions, visible in the 150-km echoes every day. Take a closer look at Figure 1 with data from 14 April 2015. Most obvious are the wide gaps in the necklace: one (marked with red) dips down to ~140 km at local noon, and a second gap at higher altitudes (marked in cyan) dips down to ~165 km. Another wide gap (marked in yellow) emerges at lower altitudes in the afternoon ascending from 140 to 160 km. Comparison with VIPIR data lets us assign approximate plasma frequencies to each of these wide gaps. In ascending order we estimate that these wide gaps correspond to plasma frequencies of approximately 3.9 MHz (yellow), 4.5 MHz (red), and 5.1 MHz (cyan). (For days with lower overall ionization, we find also a wide gap for 3.3 MHz.) First, we use these plasma frequency values only as labels for the sequence of wide gaps. Equivalently, we could label them with yellow, red and cyan. Following the VIPIR comparisons shown above, we assign the line above the red gap to 4.68 MHz and infer that the plasma frequency at the red gap is below 4.68 MHz, the plasma frequency at the cyan gap is above 4.68 MHz, and the plasma frequency at the yellow gap is much

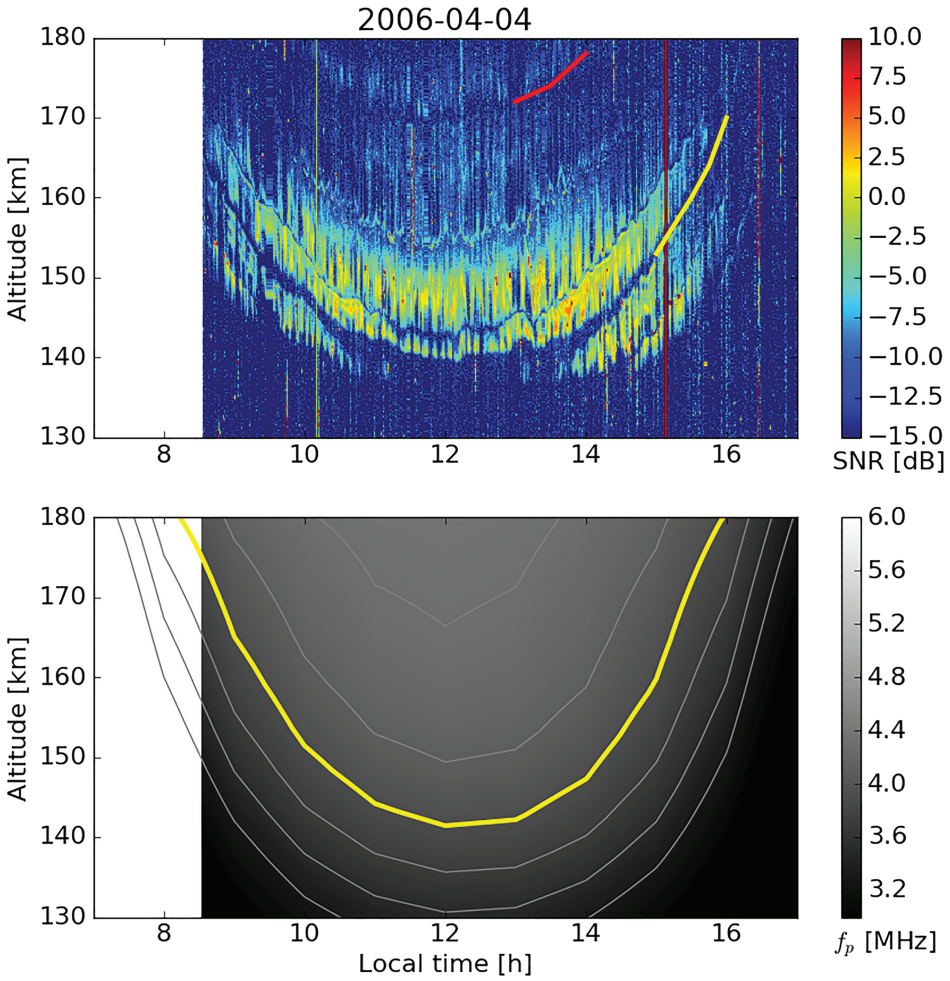

Figure 4. (top) The 150-km echoes for 14 April 2014 with major gaps marked. These are the same data as in Figure 1, but with 1-min resolution. (bottom) WACCM-X 2.0 electron densities (expressed as plasma frequency) for the same day. The 3.9- and 4.5-MHz contours are marked in yellow and red, respectively. Thin contours are spaced every 0.2 MHz.

below 4.68 MHz. We also note that between each set of wide gaps are exactly two narrow features dividing the necklace into sets of three broad and highly structured echo layers. For a more precise analysis, we plan to match small wave features of all lines and gaps to specific VIPIR frequencies as has been done by Reyes (2017) for frequency 4.68 MHz and for a 90-min interval. Second, it must be emphasized that not every day the same number of gaps is visible; sometimes only one. However, examining the necklace pattern from 2005 to 2017, spanning more than one solar cycle, allows us to keep track of the assigned plasma frequencies (or equivalent densities).

Tracking the height of wide gaps was significantly aided by comparison of plasma frequency contours provided by WACCM-X 2.0 model data as described above. Here we first show two examples (Figures 4 and 5). The first example shows data from 14 April 2015, near solar maximum conditions. These are the same data as shown in Figure 1, but with 1-min resolution. Three wide gaps are visible: yellow, red, and cyan. The plasma frequency contours below resemble closely the necklace pattern suggesting that the gap lines represent specific plasma densities.

As a second example we show also data from April, but from 4 April 2006, about 3 years before the deep solar minimum. Comparison with WACCM-X data suggests that the yellow gap (3.9 MHz) is found at lower altitudes corresponding to lower overall plasma densities. The red gap is barely visible above 170 km. Note how the thinner lines above the yellow gap are spaced much wider suggesting lower densities. A similar wide spacing of contours is seen in the model data.

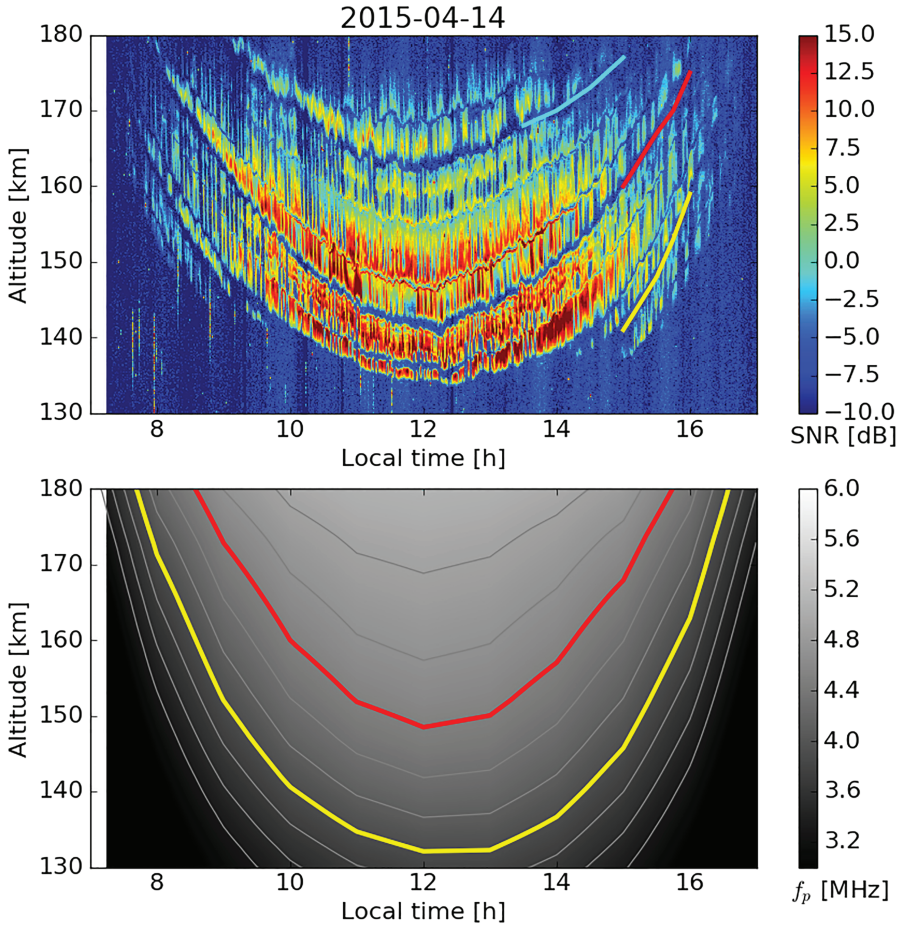

Figure 5. Same as previous figure, but for 4 April 2006. Only the 3.9-MHz contour is visible as plasma densities were lower.

3.3. WACCM-X Comparisons

We have already shown in the previous section detailed comparisons of the 150-km necklace pattern with WACCM-X 2.0 electron densities for two days spaced far apart in the solar cycle. Figure 6 shows the height of yellow, red, and cyan gaps at local noon (1200 LT) for most days with high-resolution data between 2005 and 2017, where those gaps could be identified. There are two clusters of observations with more data points: for years 2005 and 2006 and again for years 2014 and 2015. Only few observation days are available between these years and after January 2016 (see Table 1). Red and yellow gaps were at greater heights in 2005–2006, corresponding to lower electron densities, and at lower heights in 2014-2015, during the solar maximum.

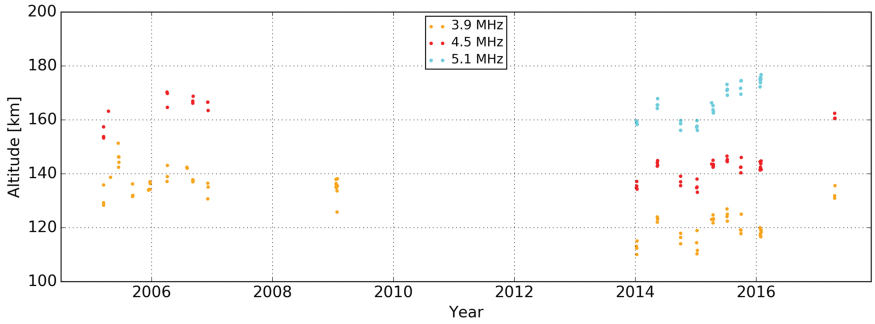

Figure 6. Height of gap location at local noon for all available echo data between 2005 and 2017. Some lower gap lines were interpolated below the lowest extent of the echoes.

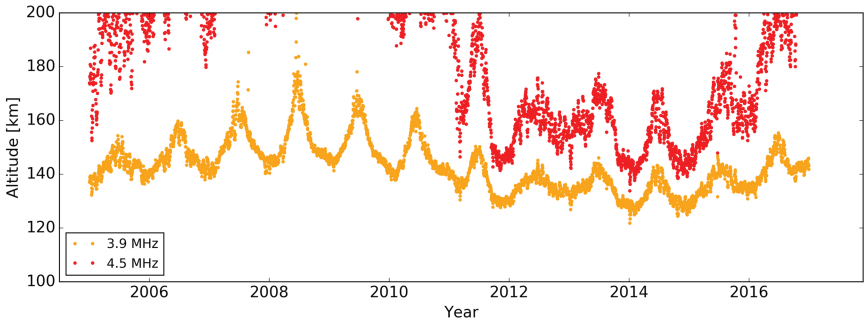

Figure 7. Heights where WACCM-X 2.0 plasma frequency is 3.9 and 4.5 MHz at local noon. Data from 2005 through 2016 are shown.

Note how the 2017 gap heights increase again. It must be mentioned that the yellow gaps were not always present at local noon since the echoes exhibit a sharp lower cutoff height, typically near 135 km (see Figures 4 and 5). In these cases (mainly for 2014–2016) we have interpolated the height at local noon with a third-order polynomial fit between morning and afternoon data.

Figure 7 displays on the same axes the heights of plasma densities 3.9 and 4.5 MHz at Jicamarca 1200 LT (1700 UT) from the WACCM-X 2.0 model run. Data points for 3.9 MHz (yellow) show a similar solar cycle trend as 150-km gaps as expected, with greatest heights during solar minimum (2009) and lowest heights during solar maximum (2015). On top of this solar cycle variation is a strong annual cycle with sharp maxima during June solstice (winter solstice at Jicamarca). While available data for gap heights in Figure 6 are relatively sparse, this annual trend with relative maxima during the middle of the year can also be recognized during 2005, 2006, 2014, and 2015. Returning to Figure 7, we see that the red data points for 4.5 MHz are generally much higher than the red gap heights. This can be interpreted as further evidence that WACCM-X 2.0 F region electron densities are too low. (A newer version (2.1) has recently become available, which generates higher densities above ~160 km but does not alter the major results and conclusions of this study.)

It should be pointed out that several seasonal studies of echo power and occurrence were performed using radars with lower power at different locations (Chau & Kudeki, 2006; Patra et al., 2017; Tsunoda & Ecklund, 2004). Here we look at gap heights which have been precisely observed with the high-power Jicamarca radar. Observations with lower-power radars are likely biased toward strong coherent backscatter from FAIs which are embedded in the majority of weaker echoes (Chau & Kudeki, 2013). While gap heights show a clear solar dependence, occurrence probability of FAIs may follow different patterns and have no clear seasonal or solar cycle pattern.

4. Discussion

Our observations strongly suggest that wide gaps in the necklace pattern occur in a systematic manner both vertically and over the solar cycle. Varying ionizing ultraviolet radiation is the main factor determining lower F region plasma densities. Furthermore, the close correspondence of the shape of the diurnal echo pattern with VIPIR virtual heights for specific plasma frequencies suggests that the quasi-parallel features represent the locations of specific plasma densities.

The wide gaps at systematically increasing plasma frequencies are most intriguing. Apparently, at these frequencies the plasma irregularities that must be responsible for the highly aspect sensitive enhanced backscatter (Chau & Kudeki, 2013) are strongly suppressed or do not form at all. While we do not have the exact frequencies (or frequency range) for the gaps, based on the comparisons with VIPIR and WACCM-X, we estimate that the wide gaps occur near 3.3, 3.9, 4.5, and 5.1 MHz.

These plasma frequencies are very similar to the condition for double resonance where the upper hybrid frequency $f_{UH}^2 = f_p^2 + f_{Be}^2$ equals integer multiples of the electron cyclotron frequency (or gyrofrequency), $n \cdot f_{Be} = n \cdot eB/(2\pi m)$. Here, the plasma frequency squared is $f_p^2 = N_e e^2/(4\pi^2 m \epsilon_0)$, where N_e, m, e, are the

electron number density, electron mass, and electron charge, respectively. This condition is expressed with the plasma frequency as

$$f_p = \sqrt{n^2 - 1} \cdot f_{Be} \tag{1}$$

For a value of $B = 2.33 \times 10^{-5}$ T at Jicamarca at 150 km (International Geomagnetic Reference Field, IGRF, Thébault et al., 2015), we find $f_{Be} = 0.652$ MHz and values for f_p and for $n = 5, 6, 7, 8$ of 3.19, 3.86, 4.52, and 5.18 MHz, which are very close to the values where we observe the wide gaps in the echoes.

In ionospheric HF heater experiments magnetic field-aligned plasma irregularities at meter scales (striations) are formed (and observed by VHF radar) at levels where the pumping frequency equals the upper hybrid frequency (see reviews by, e.g., Gurevich, 2007; Robinson, 1989). The energy of the pump wave is converted by thermal parametric instabilities (e.g., Kuo, 2002) into upper hybrid waves which heat the plasma thereby growing the striations, even creating thermal cavitons. If the pumping frequency is a multiple of the electron gyrofrequency, $f = n \cdot f_{Be}$ $(n \geq 3)$, the striations (and other heating related phenomena) are suppressed or eliminated due to the presence of electron Bernstein modes which collisionless dampen the upper hybrid waves (Bernstein, 1958; Honary et al., 1999; Hysell et al., 2010). This condition is also known as double resonance condition.

Now, Basu et al. (1982) predicted that photoelectrons with energies of several eV will also excite unstable upper hybrid waves in the daytime lower *F* region. These waves are predominantly generated around 150 km where most of the solar EUV flux is absorbed. Basu et al. (1982) also suggested that the upper hybrid waves could not grow below ~125 km due to neutral collisions and would be damped above ~170 km. This is a similar region where we observe 150-km echoes (Figure 1). Recently, Oppenheim and Dimant (2016) modeled the effect of photoelectrons on the lower *F* region plasma using a particle-in-cell model and suggested that photoelectrons can generate electron waves that ultimately are responsible for plasma irregularities causing the enhanced radar backscatter.

Combining these ideas with our observations of systematic gaps at double resonance conditions, it seems plausible that photoelectrons in the daytime lower *F* region generate upper hybrid waves as suggested by Basu et al. (1982), which amplify field-aligned plasma irregularities, similar to ionospheric heater experiments, and which can be observed as both strong and weak but highly aspect sensitive VHF backscatter. Furthermore, in the wide gap regions, electron Bernstein waves prevent the formation of striations, and backscatter is not observed, again consistent with ionospheric heater experiments. It should also be pointed out that regions of suppressed striations are 100–200 kHz wide, similar to the width of the gap regions (Gurevich, 2007).

There are many other features that strongly modulate the backscatter (Figure 1). Most prominent are the additional narrow lines and gaps that also follow specific plasma frequencies, such as the 4.68-MHz feature which was at the start of the comparisons with the VIPIR ionosonde data. Since these lines (marked in purple in Figure 1) seem to recur also at intervals of f_{Be}, these features may also be related to double resonances, but the damping or growth may require more finely tuned resonance conditions than in the wide gaps.

It has been long known that short-period gravity waves also strongly modulate the backscatter of 150-km echoes (Røyrvik & Miller, 1981), and therefore, they must also change the growth of field-aligned striations. Thermal fluctuations across the steep electron density gradient in the lower *F* region may grow into regions of significant electron depletions, similar as ionospheric heating induces depletions (Kelley et al., 1995). It seems possible that gravity waves may induce regions that now match the double resonance condition and become void of striations and backscatter. Alternative modulation processes have been suggested by Kudeki and Fawcett (1993) and Tsunoda and Ecklund (2000).

In this discussion we note that few direct observations of electron density using sounding rockets exist, which have shown only very small levels of meter-scale fluctuations above the equatorial electrojet and which decreased with altitude (Prakash et al., 1969; Smith & Royrvik, 1985). It was suggested that observations could be reconciled when taking into account the angle that the electron probe was intersecting the presumably horizontally aligned wave structures. Future in situ experiments are needed to verify these observations, to find evidence for larger and smaller fluctuations reflecting strong and weak echoes and a marked change in fluctuations where the gaps in radar echoes are observed.

5. Summary and Conclusions

We examined high-resolution 150-km echoes observed with the Jicamarca radar between 2005 and 2017. Our results are summarized as follows:

1. Simultaneously observed VIPIR ionosonde virtual height traces for 4.68 MHz correspond to a certain sharp line in the diurnal necklace pattern. This has been demonstrated for seven days of data in 2015 and 2016 (Figures 2 and 3). Further, still preliminary examination of VIPIR data suggests that also other quasi-parallel gaps and lines in the necklace pattern correspond to specific local electron densities.
2. We estimate that the major wide gaps in the necklace pattern coincide with certain, systematically increasing plasma frequencies, namely, 3.3, 3.9, 4.5, and 5.1 MHz. Comparisons of gaps with WACCM-X 2.0 data show strong similarities in diurnal patterns of gap height, gap distance, and contours of modeled plasma frequency. This further strengthens the finding that gaps are locations of specific plasma frequencies.
3. Comparisons of the entire data set with WACCM-X 2.0 plasma densities spanning more than one solar cycle exhibit systematic behavior on annual and decadal time scales according to the expected variation of solar EUV radiation as primary source of ionization. While 150-km echoes appear in the same altitude band showing little seasonal or solar cycle dependence, the specific gaps (representing fixed electron density) actually wander systematically through the region, being highest at solar minimum and lowest at solar maximum.
4. The estimated plasma frequencies for the gaps are near integer multiples of the electron cyclotron frequency with $n = 5, 6, 7, 8$, or rather, at the double resonance condition, where the upper hybrid frequency equals these integer multiples. This suggests that upper hybrid waves may play an important role in generating the FAIs, since such waves would be strongly suppressed under the double resonance condition inside the gaps and enhanced radar backscatter is not observed.

The Doppler velocity of 150-km echoes has long been used as important diagnostic for equatorial plasma drifts and electric fields (Kudeki & Fawcett, 1993). If indeed gaps and lines in 150-km echoes represent specific electron densities, then these features may also serve as powerful diagnostic to evaluate coupled neutral-ionosphere models such as WACCM-X, may help with the retrieval of ionosonde profiles in the valley region, and may be used to improve empirical models for the low-latitude ionosphere.

Acknowledgments
G. Lehmacher was supported by NSF Grant AGS-1143514. H. Wu was supported by NSF-CAREER Grant 1753214 and NASA Grant 80NSSC19K0258. E. Kudeki and P. Reyes were supported by NSF Grant AGS-1143523. D. Hysell was supported by NSF Grant AGS-1634014. The Jicamarca Radio Observatory is a facility of the Instituto Geofísico del Perú operated with support from the NSF Grant AGS-1433968 through Cornell University. The WACCM-X model is provided by NCAR, and data are available online (at https://www.earthsystemgrid.org/). The digitized gaps for all days and frequencies and other data shown in Figures 2– 7 are available in a public data repository (under https://osf.io/mcs5w/). The authors have stated no conflicts of interest. We thank the staff of the Jicamarca Radio Observatory for their excellent work in operating the radar and collecting data. Abhishek Desai and Benjamin Buck helped with digitizing the gap heights from the range-time-intensity diagrams. The authors appreciate helpful discussions with Jorge Chau about echo statistics and Nick Pedatella and Hanli Liu about the interpretation of WACCM-X results.

References

Balsley, B. B. (1964). Evidence of a stratified echoing region at 150 kilometers in the vicinity of the magnetic equator during daylight hours. *Journal of Geophysical Research*, *69*(9), 1925–1930.

Basu, B., Chang, T., & Jasperse, J. R. (1982). Electrostatic plasma instabilities in the daytime lower ionosphere. *Geophysical Research Letters*, *9*(1), 68–71.

Bernstein, I. B. (1958). Waves in a plasma in a magnetic field. *Physical Review*, *109*, 10–21.

Bullett, T., Malagnini, A., Pezzopane, M., & Scotto, C. (2010). Application of Autoscala to ionograms recorded by the VIPIR ionosonde. *Advances in Space Research*, *45*, 1156–1172.

Chau, J. L. (2004). Unexpected spectral characteristics of VHF radar signals from 150-km region over Jicamarca. *Geophysical Research Letters*, *31*, L23803. https://doi.org/10.1029/2004GL021620

Chau, J. L., & Kudeki, E. (2006). Statistics of 150-km echoes over Jicamarca based on low-power VHF observations. *Annales Geophysicae*, *24*(5), 1305–1310.

Chau, J. L., & Kudeki, E. (2013). Discovery of two distinct types of equatorial 150 km radar echoes. *Geophysical Research Letters*, *40*, 4509–4514. https://doi.org/10.1002/grl.50893

Chau, J. L., Woodman, R. F., Milla, M. A., & Kudeki, E. (2009). Naturally enhanced ion-line spectra around the equatorial 150-km region. *Annales Geophysicae*, *27*, 933–942.

Choudhary, R. K., St.-Maurice, J.-P., & Mahajan, K. K. (2004). Observation of coherent echoes with narrow spectra near 150 km altitude during daytime away from the dip equator. *Geophysical Research Letters*, *31*, L19801. https://doi.org/10.1029/2004GL020299

de Paula, E. R., & Hysell, D. L. (2004). The São Luís 30 MHz coherent scatter ionospheric radar: System description and initial results. *Radio Science*, *39*, RS1014. https://doi.org/10.1029/2003RS002914

Gelaro, R., McCarty, W., Suárez, M. J., Todling, R., Molod, A., Takacs, L., et al. (2017). The Modern-Era Retrospective Analysis for Research and Applications, Version 2 (MERRA-2). *Journal Climate*, *30*(14), 5419–5454.

Gurevich, A. V. (2007). Nonlinear effects in the ionosphere. *Uspekhi Fizicheskikh Naukri*, *177*(11), 1145–1177.

Honary, F., Robinson, T. R., Wright, D. M., Stocker, A. J., Rietveld, M. T., & McCrea, I. (1999). Letter to the Editor: First direct observations of the reduced striations at pump frequencies close to the electron gyroharmonics. *Annales Geophysicae*, *17*(9), 1235–1238.

Hysell, D. L., Nossa, E., & McCarrick, M. (2010). Excitation threshold and gyroharmonic suppression of artificial E region field-aligned plasma density irregularities. *Radio Science*, *45*, RS6003. https://doi.org/10.1029/2010RS004360

Kelley, M. C., Arce, T. L., Salowey, J., Sulzer, M., Armstrong, W. T., Carter, M., & Duncan, L. (1995). Density depletions at the 10-m scale induced by the Arecibo heater. *Journal of Geophysical Research*, *100*(A9), 17,367–17,376.

Kudeki, E., & Fawcett, C. D. (1993). High resolution observations of 150 km echoes at Jicamarca. *Geophysical Research Letters*, *20*(18), 1987–1990.

Kudeki, E., Fawcett, C. D., Ecklund, W. L., Johnston, P. E., & Franke, S. J. (1998). Equatorial 150-km irregularities observed at Pohnpei. *Geophysical Research Letters*, *25*(21), 4079–4082.

Kuo, S. P. (2002). Oscillating two-stream instability in ionospheric heating experiments. *Physics of Plasmas*, *9*(4), 1456–1459.

Lehmacher, G. A., Kudeki, E., Akgiray, A. H., Guo, L., Reyes, P. M., & Chau, J. L. (2009). Radar cross sections for mesospheric echoes at Jicamarca. *Annales Geophysicae*, *27*(7), 2675–2684.

Lehmacher, G. A., Kudeki, E., Reyes, P. M., Lee, K., Heale, C. J., & Snively, J. B. (2019). Gravity wave ducting observed in the mesosphere over Jicamarca, Peru. *Journal of Geophysical Research: Atmospheres*, *124*, 5166–5177. https://doi.org/10.1029/2019JD030264

Li, G., Ning, B., Patra, A. K., Abdu, M. A., Chen, J., Liu, L., & Hu, L. (2013). On the linkage of daytime 150 km echoes and abnormal intermediate layer traces over Sanya. *Journal of Geophysical Research: Space Physics*, *118*, 7262–7267. https://doi.org/10.1002/2013JA019462

Liu, H.-L., Bardeen, C. G., Foster, B. T., Lauritzen, P., Liu, J., Lu, G., et al. (2018). Development and validation of the Whole Atmosphere Community Climate Model with thermosphere and ionosphere extension (WACCM-X 2.0). *Journal of Advances in Modeling Earth Systems*, *10*, 381–402. https://doi.org/10.1002/2017MS001232

Liu, H. L., Foster, B. T., Hagan, M. E., McInerney, J. M., Maute, A., Qian, L., et al. (2010). Thermosphere extension of the Whole Atmosphere Community Climate Model. *Journal of Geophysical Research*, *115*, A12302. https://doi.org/10.1029/2010JA015586

Negrea, C., Zabotin, N., Bullett, T., Fuller-Rowell, T., Fang, T.-W., & Codrescu, M. (2016). Characteristics of acoustic gravity waves obtained from dynasonde data. *Journal of Geophysical Research: Space Physics*, *121*, 3665–3680. https://doi.org/10.1002/2016JA022495

Oppenheim, M. M., & Dimant, Y. S. (2016). Photoelectron-induced waves: A likely source of 150 km radar echoes and enhanced electron modes. *Geophysical Research Letters*, *43*, 3637–3644. https://doi.org/10.1002/2016GL068179

Patra, A. K. (2011). Descending ion layer property in the Gadanki radar observations of 150 km echoes and its implication to the echoing phenomenon. *Journal of Geophysical Research*, *116*, A11322. https://doi.org/10.1029/2011JA016805

Patra, A. K., Pavan Chaitanya, P., St.-Maurice, J.-P., Otsuka, Y., Yokoyama, T., & Yamamoto, M. (2017). The solar flux dependence of ionospheric 150 km radar echoes and implications. *Geophysical Research Letters*, *44*, 11,257–11,264. https://doi.org/10.1002/2017GL074678

Patra, A. K., Yokoyama, T., Otsuka, Y., & Yamamoto, M. (2008). Daytime 150-km echoes observed with the Equatorial Atmosphere Radar in Indonesia: First results. *Geophysical Research Letters*, *35*, L06101. https://doi.org/10.1029/2007GL033130

Pedatella, N. M., Chau, J. L., Vierinen, J., Qian, L., Reyes, P., Kudeki, E., et al. (2019). Solar flare effects on 150-km echoes observed over Jicamarca: WACCM-X simulations. *Geophysical Research Letters*, *46*. https://doi.org/10.1029/2019GL084790

Prakash, S., Gupta, S. P., & Subbaraya, B. H. (1969). Irregularities in the equatorial E region over Thumba. *Radio Science*, *4*(9), 791–796.

Reyes, P. M. (2012). Solar-flare effects observed over Jicamarca during MST-ISR experiments (Master's thesis), Urbana, Illinois.

Reyes, P. (2017). Study of waves observed in the equatorial ionospheric valley region using Jicamarca ISR and VIPIR Ionosonde (Doctor of Philosophy).

Richmond, A. D., Ridley, E. C., & Roble, R. G. (1992). A thermosphere/ionosphere general circulation model with coupled electrodynamics. *Geophysical Research Letters*, *19*(6), 601–604.

Robinson, A. R. (1989). The heating of the high latitude ionosphere by high power radio waves. *Physics Reports*, *179*(2), 79–209.

Roble, R. G., Ridley, E. C., Richmond, A. D., & Dickinson, R. E. (1988). A coupled thermosphere/ionosphere general circulation model. *Geophysical Research Letters*, *15*(12), 1325–1328.

Røyrvik, O., & Miller, K. L. (1981). Nonthermal scattering of radio waves near 150 km above Jicamarca, Peru. *Journal of Geophysical Research*, *86*(A1), 180–188.

Smith, A. K., Pedatella, N. M., Marsh, D. R., & Matsuo, T. (2017). On the dynamical control of the mesosphere-lower thermosphere by the lower and middle atmosphere. *Journal of the Atmospheric Sciences*, *74*(3), 933–947.

Smith, L. G, & Royrvik, O. (1985). Electron-density irregularities in the day-time equatorial ionosphere. *Journal of Atmospheric and Terrestrial Physics*, *47*(8), 813–824.

Thébault, E., Finlay, C., Beggan, C., Alken, P., Aubert, J., Barrois, O., et al. (2015). International geomagnetic reference field: The 12th generation. *Earth, Planets and Space*, *67*(1), 79.

Tsunoda, R. T., & Ecklund, W. L. (2000). On the nature of 150-km radar echoes over the magnetic dip equator. *Geophysical Research Letters*, *27*(5), 657–660.

Tsunoda, R. T., & Ecklund, W. L. (2004). On a summer maximum in the occurrence frequency of 150 km (F1) radar echoes over Pohnpei. *Geophysical Research Letters*, *31*, L06810. https://doi.org/10.1029/2003GL018704